RESEARCH ARTICLE

small methods
www.small-methods.com

Reconstructing the 3D Coordinates of Guest:Host OLED Blends with Single Atom Resolution

Lachlan Packman, Bronson Philippa, Almantas Pivrikas, Paul L. Burn, and Ian R. Gentle**

The performance of electronic and semiconductor devices is critically dependent on the distribution of guest molecules or atoms in a host matrix. One prominent example is that of organic light-emitting diode (OLED) displays containing phosphorescent emitters, now ubiquitous in handheld devices and high-end televisions. In such OLEDs the phosphorescent guest [normally an iridium(III)-based complex] is typically blended into a host matrix, and charge injection and transport, exciton formation and decay, and hence overall device performance are governed by the distribution of the emissive guest in the host. Here high-angle annular dark-field scanning transmission electron microscopy (HAADF-STEM) is used with depth sectioning to reconstruct the 3D distribution of emissive iridium(III) complexes, *fac*-tris(2-phenylpyridine)iridium(III) [Ir(ppy)$_3$], blended into the amorphous host material, tris(4-carbazoyl-9-ylphenyl)amine (TCTA), by resolving the position of each single iridium(III) ion. It is found that most Ir(ppy)$_3$ complexes are clustered with at least one other, even at low concentrations, and that for films of 20 wt.% Ir(ppy)$_3$ essentially all the complexes are interconnected. The results validate the morphology of blend films created using molecular dynamics simulations which mimic the evaporation film-forming process and are also consistent with the experimentally measured charge transport and photophysical properties.

1. Introduction

1.1. Morphology of Guest:Host Blends

In a number of areas of technology, the 3D distribution of guest molecules or atoms in a host matrix is critical to the performance of the device, particularly in technologies that contain organic semiconductors and perovskites, as well as separators and solid-electrolyte interphases in batteries amongst many others. Efficient organic light-emitting diodes (OLEDs) fabricated using evaporation-based techniques are composed of multiple layers with the key emissive layer comprising a guest-host blend. It has been generally assumed that as the concentration of the light-emitting guest is low in the emissive layer, the evaporative process leads to films in which the guest is evenly distributed throughout the film.[1] However, in the cases where the guest-host blend films are essentially amorphous and both components are of similar chemical nature (e.g., with respect to electron density), it is difficult to probe the film structure experimentally. That is, a key issue in such studies is the ability to have sufficient contrast between the components in the film. Furthermore, many experimental techniques that are used to study film morphology only provide an average of the ensemble of molecular distribution within the film. For example, neutron reflectometry studies of *fac*-tris(2-phenylpyridine)iridium(III) [Ir(ppy)$_3$] in deuterated 4,4′-bis(carbazol-9-yl)biphenyl [CBP] (in which the deuterated host provides the contrast with the guest) showed that the Ir(ppy)$_3$ molecules were, on average, evenly distributed through the depth of the film.[2] However, reflectometry only provides information in the direction normal to the interface, and there are clear inferences from indirect experimental methods that there are intermolecular interactions between guest molecules within the host. For example, decreases in the photoluminescence (PL) quantum yield (PLQY) or lifetimes of blends can indicate that the emissive species are interacting. Given the difficulty of experimentally determining the location of the molecules at atomic resolution, there have now been a number of reports of molecular dynamics simulations developed for mimicking guest-host film formation.[3–6] One of the most realistic

L. Packman, P. L. Burn, I. R. Gentle
Centre for Organic Photonics & Electronics (COPE)
School of Chemistry and Molecular Biosciences
The University of Queensland
Brisbane, QLD 4072, Australia
E-mail: p.burn2@uq.edu.au; i.gentle@uq.edu.au

B. Philippa
College of Science & Engineering
James Cook University
Townsville, QLD 4814, Australia

A. Pivrikas
Physics Department
Murdoch University
Perth, Western Australia 6150, Australia

The ORCID identification number(s) for the author(s) of this article can be found under https://doi.org/10.1002/smtd.202301305

DOI: 10.1002/smtd.202301305

simulation methods for mimicking the evaporation process has led to simulated $Ir(ppy)_3$:TCTA blend film morphologies that were consistent with the measured photophysical and charge transport properties of the films.[5] However, to date, there has not been a systematic study experimentally mapping the position of the guest in the host at different concentrations to directly validate the simulated film morphologies.

OLED emissive layers that contain heavy metal complex emitters provide an opportunity to validate the simulated film morphologies directly, as the electron density associated with the metal is significantly higher than the associated ligands and host material. High-angle annular dark field scanning transmission electron microscopy (HAADF-STEM) can in principle be used to identify the location of metal atoms in an organic matrix. We are aware of only a single report of the use of HAADF-STEM for studying the location of the metal complexes in phosphorescent emissive films.[1] The report showed HAADF-STEM images of a 10 wt.% $Ir(ppy)_3$:TCTA blend and it was found that the guests were not homogeneously distributed but could aggregate. However, it was unclear from the report whether the observed clusters were simply on the surface of the film or throughout its bulk.

In this manuscript, we report a HAADF-STEM method that can be used to determine the 3D distribution of phosphorescent emissive guests within an OLED emissive layer blend with atomic resolution. We describe the experimental process required to give the depth profile as well as the analysis method that enables visualization of the location of the emissive guests. Evaporated films composed of blends of $Ir(ppy)_3$ in TCTA with guest concentrations of 1, 6, 10, and 20 wt.% were used to develop and demonstrate the method. Finally, we compare the distribution of the $Ir(ppy)_3$ guest molecules with the simulated film morphologies of the same materials and blend ratios and discuss how it relates to observed experimental properties.

2. Results and Discussion

2.1. Single Atom Resolution with HAADF-STEM

To investigate $Ir(ppy)_3$ guest distribution within the TCTA host, 10 nm thick films were evaporatively deposited onto pure silicon transmission electron microscopy grids (see Methods section). The films were formed using co-evaporation with the guest:host ratio varied between 1 and 20 wt.% based on the relative evaporation rates of the two materials. Imaging of the blended films was performed on a Cs-corrected Hitachi HF5000 (>78 pm resolution in STEM mode). The combination of the spatial resolution and the atomic number contrast of the signal from the HAADF detector of this instrument enabled the distinguishing of the guest from the host by imaging the iridium(III) ion at the center of an $Ir(ppy)_3$ complex. It is important to note that in the raw experimental data, the regions of high electron density (greatest intensity) in HAADF-STEM images would typically be pictured as white spots on a dark background. However, all the HAADF-STEM images in this manuscript are shown inverted for clarity, as it is easier to visualize a relatively smaller number of black images on a white background. **Figure 1a** is a HAADF-STEM image of a 10 wt.% $Ir(ppy)_3$:TCTA blend film generated from a series of horizontal beam scans from the top of the image to the bottom. The scan time used to collect the image was 10 s. It is immediately apparent that there are small dark spots within the image, ranging from dark grey (almost black) to much lighter shades, which arise from the iridium(III) ions in the center of the complexes. The range of spot intensities (grey scale) observed arises, at least in part, from the iridium(III) ions being located at different depths within the film, which will be discussed in more detail later. The pixel size in these images is 0.024 nm and based on the diameter of an iridium(III) ion being 0.164 nm, a single iridium(III) ion appears as a series of spots encompassing 7 pixels.[7] Figure 1b illustrates a single iridium(III) ion (underlined in red) in the region highlighted by the red box in Figure 1a. The zoomed-in view of Figure 1b illustrates the individual pixels making up an iridium (III) ion and confirms the single-atom resolution of the measurement. The key point from Figure 1a is that when $Ir(ppy)_3$ is at a concentration of 10 wt.% in TCTA, the complexes exist both as separate isolated complexes as well as aggregated clusters of various sizes. Note that this is a frozen image of the features, whereas it is understood that the regions of high electron density are not static (see Video S1, Supporting Information) and show statistical movement, although the average net displacement of electron-dense regions is zero. The movies in Video S1 (Supporting Information) are drift corrected, meaning that the net displacement of electron-dense regions between subsequent frames has been corrected during image processing. This drift is not due to the $Ir(ppy)_3$ complexes diffusing but is, at least in part, a result of experimental factors such as thermal fluctuations, vibrations, stage movement and magnetic field effects.

As HAADF-STEM is a transmission technique, the overlap of multiple iridium(III) ions occupying the same lateral coordinates but at different depths results in an increase in the number of scattering events and thus intensity in the HAADF-image. Furthermore, weaker scattering from the many carbon atoms of the host and ligands of the complex also contributes to the observed background signal. The fact that a number of scattering events occur is confirmed by the image generated using the secondary electron (SE) detector (essentially a scanning electron microscopy (SEM) image with single atom resolution) (Figure 1c). It is important to note that the SE detector collects both the secondary electrons and additionally, the backscattered electrons, which enhances the electron density contrast in the image. The images in Figure 1a,c were collected in parallel on the same section of the film and are consistent, with the region in the HAADF-STEM that has the highest number of iridium(III) ions also having the highest electron density in the SEM image. As with the HAADF-STEM images, the SEM image was contrast inverted and therefore the high electron-dense regions appear as black spots. Finally, it should be noted that the SEM measurement has less depth information and arises mainly from iridium(III) atoms on or near the surface of the film.

It is clear from Figure 1 that we can identify individual iridium(III) ions using HAADF-STEM. Given that the iridium(III) ions (diameter = 0.16 nm) are at the center of the *facial* complex (diameter = 1.2 nm) we can use this information to determine how close the complexes are within the film. The initial analysis was done on the $Ir(ppy)_3$ complexes within ≈5 nm of the surface of the film (shown in Figure 1a). To illustrate the proximity of complexes, circular outlines with diameters of 1.2 nm were superimposed around each of the iridium(III) atoms in the HAADF-STEM image (Figure 1d). It is clear from this

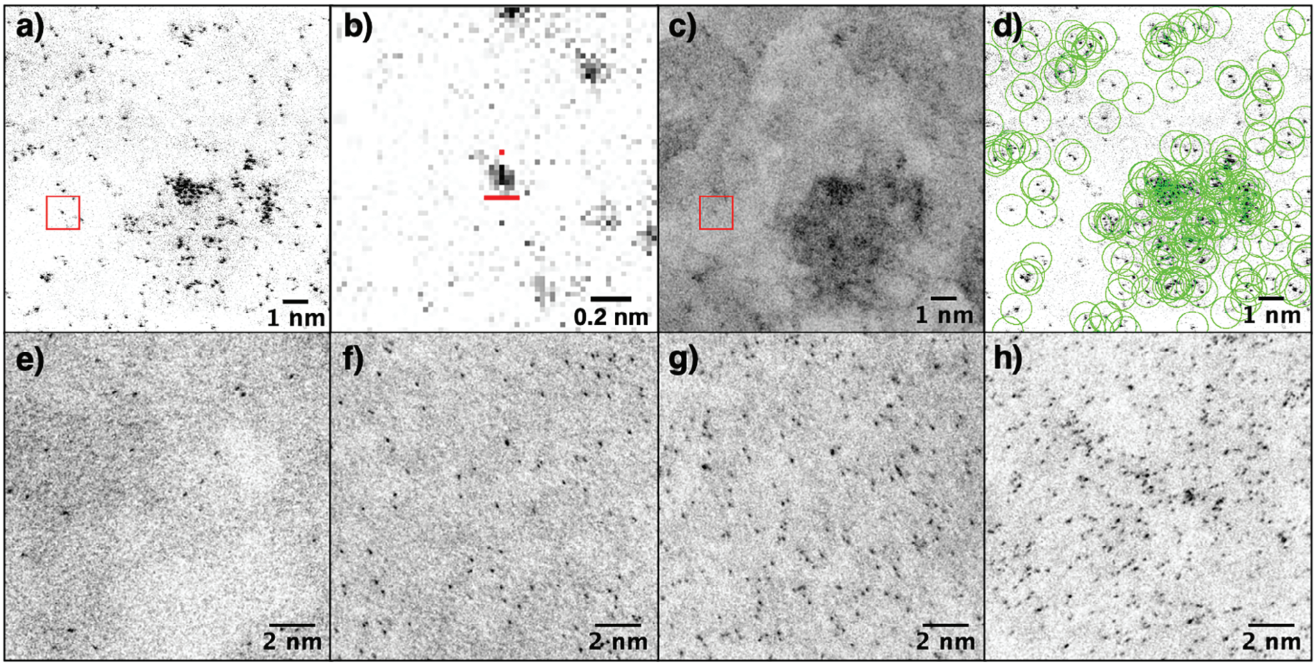

Figure 1. a) HAADF-STEM image of a 10 wt.% $Ir(ppy)_3$:TCTA blend film. Highlighted in the red box is a single iridium(III) ion. b) A zoomed-in image of the image of the red box. The red square depicts one pixel with a 0.024 nm width and the red line shows the expected iridium (III) ion diameter. c) is the SEM image captured simultaneously with the HAADF-STEM image, with the red box capturing the same iridium(III) ion that is near the surface of the film. d) Superimposed circles with 1.2 nm diameter (with a green outline) showing the approximate size of the $Ir(ppy)_3$ complexes. e–h) Single frames from the through-focus series of films with 1, 6, 10, and 20 wt.% respectively $Ir(ppy)_3$:TCTA blend films. There is an increased background signal in these images as the image-capturing parameters were optimized for minimum capture time. HAADF-STEM and SEM contrasts are inverted for clarity. That is, greater electron density corresponds to a darker part of the plot.

2D analysis that there is spatial overlap between the complexes. This apparently unphysical overlap can arise from two sources. First, the crystal structure of $Ir(ppy)_3$ shows the closest iridium-iridium ion distance is 0.77 nm, which is a result of the ligands intercalating.[8] It is interesting to note that results from a radial distribution function of a simulated amorphous blend of $Ir(ppy)_3$ in TCTA show the iridium-iridium ion distance can be as small as 1.0 nm.[5] The second source of the significant overlap arises from the depth of field in the measurement. The small condenser aperture used to achieve high lateral resolution in STEM mode with an aberration-free probe results in poor vertical resolution and a large depth of field (in this case ≈5 nm), which is much larger than the lateral resolution.[9,10] Thus, within the depth of field of the measurement it is possible to have up to five iridium(III) ions in focus in a vertical direction so that while it may appear that two iridium(III) ions are adjacent, they may be vertically separated but within 5 nm due to the depth of focus of the measurement. Therefore, to accurately determine clustering and aggregation, a procedure is required to achieve better vertical resolution, which is discussed in the next section.

2.2. Depth Sectioning Single Ions in an Amorphous Matrix

One method to achieve depth resolution is to use a larger aperture, which widens the convergence angle and leads to a reduction in the depth of field, enabling a thin slice of the film to be imaged. However, this limits the volume of the film that can be analyzed in a single image. The alternative is to keep the same aperture but take a series of images where the focus of the beam is at different depths in the film (see Video S2, Supporting Information). Each iridium(III) ion can therefore be represented as a function of the focal depth where the brightness of the ion diminishes as the distance between it and the focal plane increases. That is, the brightness of an iridium(III) ion is at its maximum when the focal plane is closest to the depth of the ion within the film. We used the latter method where the focal plane depth was varied in 0.2 nm steps between the upper film surface and the substrate. An example of the depth sectioning approach for a 10 nm thick 6 wt.% $Ir(ppy)_3$:TCTA blend film is shown in **Figure 2**. Movies of the through-focus series and the 3D projection for the 6 wt.% $Ir(ppy)_3$:TCTA blend film are shown in Videos S1 and S2 (Supporting Information). The method was also used to analyze the 1, 10, and 20 wt.% films. The through-focus series of HAADF-STEM images for the 6 wt.% $Ir(ppy)_3$:TCTA film (Figure 2) consists of 18 frames. It is important to note that the lateral resolution deteriorates as the objective focus is changed, and so the full 10 nm depth could not be measured.

Figure 2a is a projection of all 18 images layered on top of each other. The iridium(III) ions in the projection appear not as single points but as collections of points in the lateral direction, which arises from the thermal motion of the iridium(III) ions. Figure 2b is a single frame (13) of the through-focus series, corresponding to a depth of 2.4 nm. What is important to note for this image is that not all the iridium(III) ions observed in the composite of the

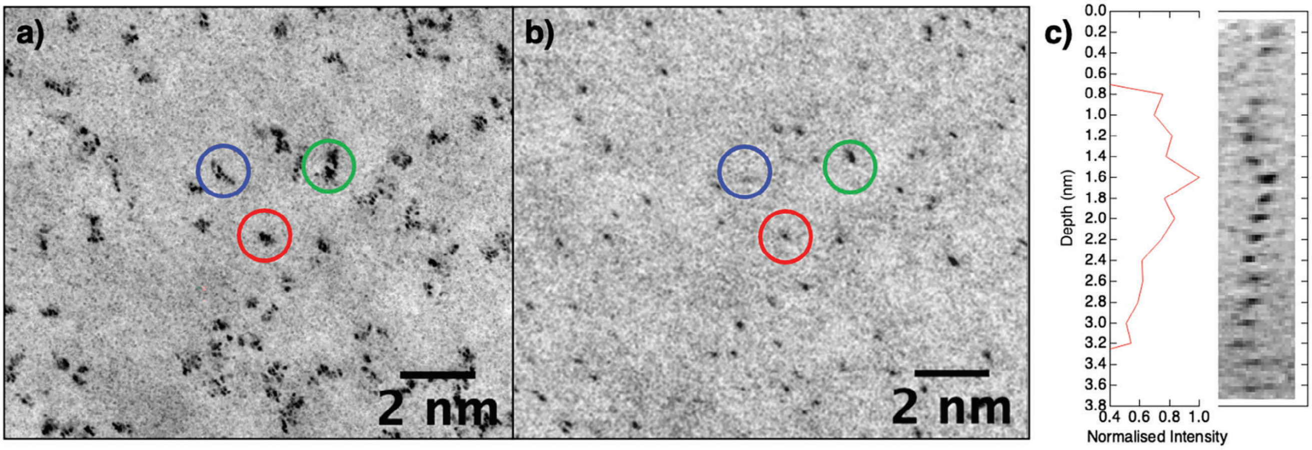

Figure 2. a) Composite of all 18 HAADF-STEM images from the through-focus series of the 6 wt.% $Ir(ppy)_3$:TCTA film. b) Single frame eight from the through focus series. The red circle shows a single atom in focus, the blue circle shows an atom just out of focus and the green circle shows two overlapping iridium(III) ions. c) Brightness of an iridium(III) ion as a function of depth from the film surface captured by changing the focal depth. HAADF-STEM contrast inverted for clarity.

frames are observed in the single frame since, as noted earlier, the brightness of an atom depends on how far it is located from the focal plane. This provides confidence that the depth sectioning method used here is successful. An example of the ability to depth section is the fact that the iridium(III) ion within the blue circle is clearly seen in the composite image in Figure 2a but barely visible in the single frame of Figure 2b. Therefore, the iridium(III) ion in the blue circle is not at a depth of 2.4 nm within the film. A second example is the electron density highlighted in the green circle, which in Figure 2a is composed of two iridium(III) ions. The two iridium(III) ions are overlapping in Figure 2b and appear as only one spot due to the movement of the ions between frames. Regardless of the proximity of the iridium(III) ions, by depth sectioning it can be determined that they are at different vertical distances and are not interacting (as discussed in the next section). The single atom in the red circle in Figure 2a,b is plotted as a function of depth in Figure 2c. The image shows the focal depth (0.2 nm steps) versus the intensity of the signal for one iridium(III) ion. It can be seen from both the normalized intensity plot versus depth and visualization plots that there is a maximum in brightness in frame eight. Thus, the iridium(III) ion is located at a depth of 1.6 nm from the surface of the film. The visualization plot in Figure 2c also shows the thermal motion in the lateral direction of the iridium(III) ion, as the position of the iridium(III) ion is not perfectly vertical but moves laterally (left to right and vice versa) between frames.

2.3. Reconstructing the 3D Coordinates of Iridium Ions

With the method for determining the 3D location of the iridium(III) ions in hand, the next stage in the analysis was to visualize the proximity of the ions and by inference, the complexes, throughout the full depth of the film. Due to the large number of ions, we developed an automated process to analyze the image series.[11] Fiji was used to correct stage drift ($\approx$1 nm min^{-1}) that occurred between images in the series using the Stack Reg plugin, and a MATLAB algorithm was used to reconstruct the 3D coordinates.[12] For the 3D reconstruction process, the cartesian coordinates for the iridium(III) ions were extracted from the images. The positions of the iridium(III) ions were correlated between the frames and the depth in the film was determined from the intensity of the signal as a function of depth as described in the previous section. **Figure 3**a–d are the HAADF-STEM projections of the through-focus series for the 1, 6, 10, and 20 wt% $Ir(ppy)_3$:TCTA films, with Figure 3e–h the 3D reconstruction of the corresponding through-focus series of the film. Each iridium(III) ion is centered within a 1.2 nm diameter sphere to represent the volume of an $Ir(ppy)_3$ complex. It can be seen that some complexes are isolated and some are close to one or more other complexes. In order to gain a more quantitative understanding of the clustering, we used a cut-off distance of 1.4 nm between two iridium(III) ions, which had been previously used to define clusters in a report of the morphology of films containing $Ir(ppy)_3$ and TCTA formed using molecular dynamics simulations of the evaporation process, to define whether complexes were members of a cluster.[5] The cluster sizes are colored depending on the number of complexes within a cluster, so that isolated complexes are white, pairs are black, clusters of three to ten are blue, clusters of 11–100 are green and any larger are red. It can be seen that at the lowest concentration, the complexes are isolated or form small clusters. It should be noted that the ability to reconstruct the clusters is affected by variations in the noise, thickness, vertical overlap, and the movement of iridium(III) ions between images. As a result, in some cases iridium(III) complexes can be unassigned or incorrectly assigned in the reconstruction. With increasing $Ir(ppy)_3$ concentration the number and size of the clusters increases, and the analysis of these will be discussed in the next section. However, before doing so we highlight the strength of the method we have developed to determine whether the complexes are interacting or not. The green circle in Figure 3b,f corresponds to the same two iridium(III) ions in the green circle in Figure 2a,b. In Figure 2a,b it is not possible to determine whether the two ions are simply close laterally or at different depths. However, the 3D reconstruction shows that these two iridium(III) ions are in fact at different depths (1.6 nm away from each other) so

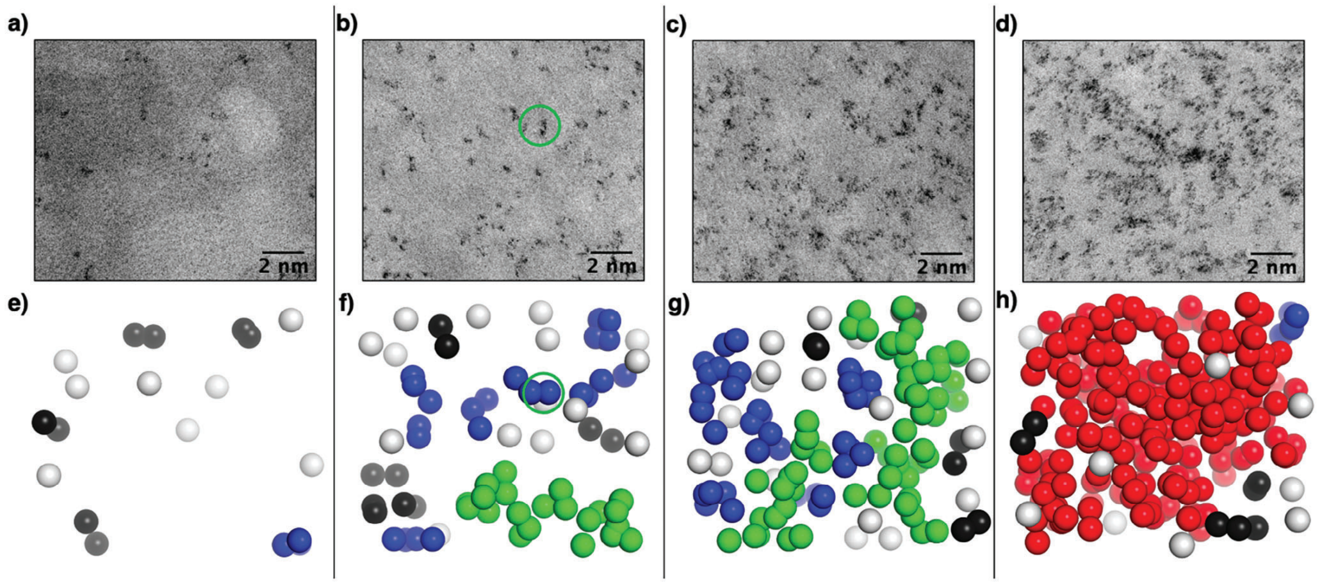

Figure 3. a–d) 2D projections of the through focus series of HAADF-STEM images for Ir(ppy)$_3$:TCTA blend films (1, 6, 10, 20 wt.%, respectively). HAADF-STEM contrast has been inverted for clarity. e–h) 3D reconstructed Ir(ppy)$_3$ distribution. The spheres are 1.2 nm in diameter. The ability to identify the positions of the iridium(III) ions within the film enables us to determine the actual concentration of the guest in the host from the number of iridium(III) ions in a selected volume of the film and the relative mass densities of the materials. In this way the actual concentrations of the films used were 2.7 wt.% Ir(ppy)$_3$ in the host (nominally 1 wt.%), 7.8 wt.% (nominally 6 wt.%), 13.5 wt.% (nominally 10 wt.%) and 25.2 wt.% (nominally 20 wt%). That is, the films contained slightly more Ir(ppy)$_3$ than expected from the experimentally measured relative evaporation rates of the two materials. To avoid confusion, the films will continue to be referred to as 1, 6, 10 and 20 wt.%, noting that the actual compositions are slightly different.

although they have very similar lateral coordinates, they are not part of the same cluster.

2.4. Cluster Analysis and Implications for Simulated Morphologies and Device Performance

In the first part of the cluster analysis, we compared the distribution of the cluster sizes as a function of concentration (**Figure 4a**) with films created using molecular dynamics simulations of the co-evaporation of Ir(ppy)$_3$:TCTA (Figure 4b). From the experimental results, the majority of the Ir(ppy)$_3$ in the nominally 1 wt.% film was clustered with only 42% (8 molecules) of Ir(ppy)$_3$ existing as isolated molecules. In the 10 and 20 wt.% films, only 22% (15 molecules) and 16% (19 molecules) of the Ir(ppy)$_3$ complexes were not clustered. Furthermore, when the Ir(ppy)$_3$ was at these higher concentrations, clusters containing over ten molecules started to form. Finally, for the 20 wt.% Ir(ppy)$_3$ films, 90% (220 molecules) of the Ir(ppy)$_3$ complexes were interconnected with only 4% (11 molecules) not forming part of the large network. The fact that the Ir(ppy)$_3$ forms clusters in the TCTA host is not unexpected as they have different shapes and significantly different physical properties such as surface energies,[3] and a propensity to be crystalline.[2] The evaporative process leads to a metastable film morphology which, depending on the thermal properties of the materials and the relative concentrations of the two components, can be stable or change over time. For example, thermally evaporated low wt.% Ir(ppy)$_3$:CBP blend films are initially amorphous, but over the course of a couple of days the films become crystalline with separated CBP and Ir(ppy)$_3$ rich re-

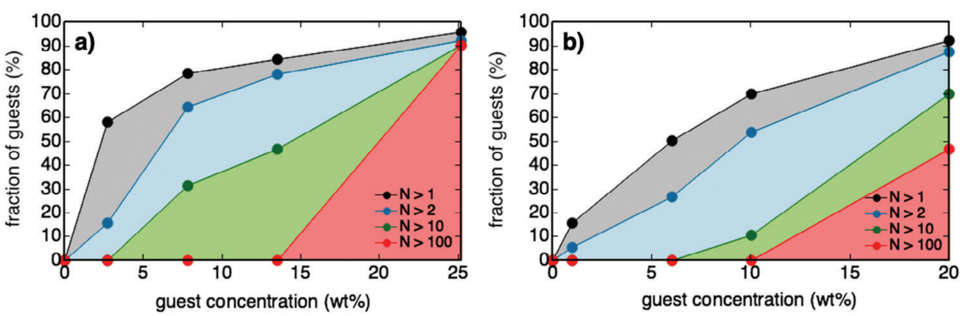

Figure 4. Cluster sizes are determined from a) the experimentally derived morphologies with the actual guest concentrations determined from the HAADF-STEM and b) morphologies calculated from molecular dynamics simulations. The white area of the graph represents the proportion Ir(ppy)$_3$ complexes not clustered, the black clusters of 2, the blue clusters of 3 up to 10, the green clusters of 11 up to 100 and the red clusters over 100. Note b) is adapted from the published graph.[5]

gions as the CBP crystallizes.[13] The trends in the experimentally determined cluster sizes are remarkably similar to those found in the simulated films, although the proportion of complexes in each cluster size is consistently greater in the experimental results. The similarity between the simulated and experimental films is encouraging, given that differences inevitably exist between the two methods of film formation, such as different deposition rates and the fact that the 10–20 ns annealing time that is used for the simulations is orders of magnitude shorter than the annealing time when fabricating a film.[5] It is also important to note that the sample volume used for the experimentally determined cluster size (13 nm × 13 nm × 5 nm) was smaller than the simulation volume (34.1 nm × 33.4 nm × 11–14 nm). However, the critical point is that the experimental film morphologies are consistent with the clustering behavior observed in the molecular dynamics simulations of the co-deposition evaporation process.

Furthermore, the experimental cluster analysis is also consistent with the photophysical and charge mobility measurements on Ir(ppy)$_3$:TCTA blend films,[5] and the characteristics of devices incorporating Ir(ppy)$_3$ guest-based emissive layers more generally. For example, the first reported Ir(ppy)$_3$ devices showed there was a strong guest concentration dependence on their performance, with devices consisting of 6 wt.% Ir(ppy)$_3$ being the most efficient and those having higher concentrations (12 wt.% and finally 100 wt.%) being over an order of magnitude less efficient.[14] One characteristic that can lead to lower device efficiencies is the presence of guest–guest interactions that can lead to quenching of the photoluminescence (PL). Measurements of the PL lifetime of films composed of Ir(ppy)$_3$ have shown that a reduction in lifetime occurs at higher guest concentrations due to close-range interactions between the guests.[15] Thus, both these results are consistent with the measured clustering reported in the current manuscript.

Finally, as commented on earlier, the concentration dependence of the PL quantum yield (PLQY) and transport of charges in Ir(ppy)$_3$:TCTA based films at similar concentrations to those we have used has been reported.[5,16] The highest PLQY was measured for films composed of 6 wt.% guest, with the value decreasing significantly toward higher guest concentrations. It was found that for PL quenching to occur the ligands of neighboring Ir(ppy)$_3$ molecules had to at least be partially overlapped (Ir-Ir distance less than 0.9 nm as Ir(ppy)$_3$ molecules have a diameter of ≈1 nm). Therefore, our experimental results validate the simulations that explained the PL quenching observed. It was also reported that the hole mobility of the neat host material (TCTA) had the highest mobility and when 1 wt.% Ir(ppy)$_3$ was blended into the film, the hole mobility was reduced by two orders of magnitude. The reason for this is that the ionization potential of Ir(ppy)$_3$ is smaller than that of the TCTA, so the guests act as a trap for holes, impeding their transport.[17] At concentrations above 10 wt.% the hole mobility was reported to increase and approach the mobility of neat Ir(ppy)$_3$, which is consistent with our HAADF-STEM results that show the Ir(ppy)$_3$ molecules clustering and forming extended pathways along which the holes could hop.

It is important to note that the effect of concentration on the photophysical and device properties is not unique to blends containing Ir(ppy)$_3$, as essentially all the efficient phosphorescent-based OLEDs fabricated using evaporative methods also only incorporate a small proportion of guest (3–12 wt.%) in the emissive layer.[18–22] Thus, the current HAADF-STEM results provide the basis for explaining previous device trends.

3. Conclusion

In summary, we have experimentally identified the 3D locations of Ir(ppy)$_3$ guest molecules blended with TCTA with single atom detail. This was achieved by taking a through-focus series of HAADF-STEM images of the iridium(III) ions at the center of the Ir(ppy)$_3$ complexes with the resolution and contrast required to resolve single ions. The technique allowed the determination of the actual concentration of the Ir(ppy)$_3$ guest molecules in the film with the TCTA host and how it compared to what was experimentally expected based on the evaporation rates of the two materials. We found that there were slightly more Ir(ppy)$_3$ molecules in the films than were predicted based on the relative evaporation rates. By changing the focal depth in 0.2 nm increments it was possible to identify the 3D coordinates of the iridium(III) ions and reconstruct the interactions of the iridium(III) complexes in the film. It was found that even at low concentrations there was significant clustering of the iridium(III) complexes and at a nominal 20 wt.% there were only a few complexes that were not part of a cluster. The experimental results were compared with the film morphology of the same materials at similar concentrations created using molecular dynamics simulations of the evaporation process. The two film morphologies were similar despite the different deposition timescales and hence the experimental results validate the simulation method and vice versa. HAADF-STEM is therefore, a powerful technique for identifying film morphology but is reliant on at least one of the components having a significantly higher electron density relative to the other components of the film.

4. Experimental Section

Film Preparation and Contamination Mitigation: High-angle annular dark field (HAADF) and secondary electron (SE) images were acquired on a Hitachi HF5000 Cs-STEM/TEM. To reduce contamination sourced from inside the microscope, the column was baked for 72 h prior to the measurements. One day prior to the measurements liquid nitrogen was added to the cold trap to condense residual contamination vapors in the column from the bake and no other samples were inserted into the microscope prior to measurements. Further liquid nitrogen was added to the cold trap 2 h prior to the measurements. Pure silicon transmission electron microscopy (TEM) windows were purchased from Electron Microscopy Sciences. *Fac*-tris(2-phenylpyridine)iridium(III) [Ir(ppy)$_3$] and tris(4-carbazoyl-9-ylphenyl)amine (TCTA) were purchased from Luminescence Technology Corp and used as received. Grids were transferred into an evaporator chamber and placed under high vacuum (<1 × 10^{-6} mbar), and Ir(ppy)$_3$ and TCTA were co-deposited at a total rate of 1.0 Å s^{-1} to a thickness of 10 nm. The individual rates were controlled so that the films were nominally composed of 1, 6, 10, or 20 wt.% of Ir(ppy)$_3$. Samples were stored under high vacuum in the evaporator prior to the measurements. To reduce contamination from the TEM holder, the holder was disassembled, washed with ethanol and plasma cleaned (E. A. Fischione 1020 Plasma Cleaner) for 5 min. Samples were transferred onto the holder and the sample loaded holder was placed under vacuum (Zone II for SEM) for 15 min prior to insertion. These collective contamination controls resulted in no contamination of the films for the duration of the experiment.

Image Acquisition: The Hitachi HF5000 was operated in STEM, HR mapping mode (second smallest spot size) with condenser aperture 4 (convergence angle ≈23 mrad). The high-angle dark field detector was operated in diffraction contrast mode. It is important to note that the samples did not diffract, therefore there was no contrast due to diffraction. This enabled more of the lower-angle scattering to be captured, which increased the signal of the iridium(III) ions in the images. Prior to the acquisition of the 3D data set, the sample was brought to the eccentric height with the stage height, the objective lens current center was aligned with the optic axis, and aberrations up to the third order were corrected. The stage was held static and was left for 30 min to minimize stage drift. In order to avoid reintroducing stage drift, only the image-shift function (ISF) and objective focus were used to adjust the field of view and focus respectively. All aberrations were corrected again, resulting in an electron probe size of less than 0.1 nm. ISF was used to shift the field of view away from the region used to correct the aberrations, as spotting the beam during the aberration correction can case beam damage in the form of a 3 nm diameter hole. To avoid deterioration of the aberration correction, ISF use was kept to a minimum. Two-fold axial astigmatism was corrected manually until the iridium (III) ions appeared as circular spots. At this point, specimen drift was less than 1 nm min^{-1}. Image acquisition was set to 512×512 pixels with 0.024 nm pixel resolution, and a 10 s slow scan (images were captured as quickly as possible). A through-focus series was acquired by capturing a HAADF image, then adjusting the focus by 0.2 nm, and repeating until the iridium(III) ions went from out of focus, to in focus, and out of focus again (data set acquisition takes several minutes).

Image Processing: Image sequences were imported into Fiji as a stack.[11] The drift in the field of view between frames in the through focal series was corrected using the Fiji plugin StackReg.[12] The image series were then cropped to remove the field of view that does not appear in all frames in the image sequence. The corrected files were then imported into MATLAB for the reconstruction of the 3D atomic coordinates (MATLAB version: 9.5.0 (R2018b), Natick, Massachusetts: The MathWorks Inc.; 2018). Several steps were used to extract the xy coordinates of the iridium(III) ions from each image: first, a Gaussian filter was added to the image to reduce noise; second, the background was subtracted with a threshold; and then the local maxima were found giving the coordinates. As the iridium(III) ions appear in multiple frames, the next step was to correlate the iridium(III) ions between neighboring frames based on proximity. The iridium(III) ion depth within the film was calculated based on the depth at which the maximum intensity occurred, as depicted in Figure 3c, generating a list of 3D atomic coordinates. For the cluster analysis, the pairwise distance between every iridium(III) ion was calculated and values under 1.4 nm were considered clustered. The 3D reconstructions and cluster analysis were depicted using PyMOL (The PyMOL Molecular Graphics System, Version 2.0 Schrödinger, LLC).

Supporting Information

Supporting Information is available from the Wiley Online Library or from the author.

Acknowledgements

The work was carried out at the Centre for Organic Photonics & Electronics at The University of Queensland. The work was supported by the Australian Research Council Discovery Program (DP210102192). The authors acknowledge the facilities, and the scientific and technical assistance, of the Centre for Microscopy and Microanalysis (CMM), The University of Queensland, (the Queensland node of Microscopy Australia). In particular, the assistance of Dr. J. Otte & Dr. J. Fernando is gratefully acknowledged. P.L.B. is a UQ Laureate Fellow.

Open access publishing facilitated by The University of Queensland, as part of the Wiley - The University of Queensland agreement via the Council of Australian University Librarians.

Conflict of Interest

There are no conflicts of interest to declare.

Data Availabiliy Statement

The data that support the findings of this study are available from the corresponding author upon reasonable request.

Keywords

blends, clustering, OLED, organic semiconductors, scanning transmission electron microscopy

Received: September 26, 2023
Revised: March 8, 2024
Published online: March 22, 2024

[1] S. Reineke, G. Schwartz, K. Walzer, M. Falke, K. Leo, *Appl. Phys. Lett.* **2009**, *94*, 163305.
[2] A. R. G. Smith, J. L. Ruggles, H. Cavaye, P. E. Shaw, T. A. Darwish, M. James, I. R. Gentle, P. L. Burn, *Adv. Funct. Mater.* **2011**, *21*, 2225.
[3] C. Tonnelé, M. Stroet, B. Caron, A. J. Clulow, R. C. R. Nagiri, A. K. Malde, P. L. Burn, I. R. Gentle, A. E. Mark, B. J. Powell, *Angew. Chem., Int. Ed.* **2017**, *56*, 8402.
[4] T. Lee, B. Caron, M. Stroet, D. M. Huang, P. L. Burn, A. E. Mark, *Nano Lett.* **2017**, *17*, 6464.
[5] M. Gao, T. Lee, P. L. Burn, A. E. Mark, A. Pivrikas, P. E. Shaw, *Adv. Funct. Mater.* **2020**, *30*, 1907942.
[6] T. Lee, A. V. Sanzogni, P. L. Burn, A. E. Mark, *ACS Appl. Mater. Interfaces.* **2020**, *12*, 40548.
[7] R. Shannon, *Acta Cryst. A.* **1976**, *32*, 751.
[8] J. Breu, P. Stössel, S. Schrader, A. Starukhin, W. J. Finkenzeller, H. Yersin, *Chem. Mater.* **2005**, *17*, 1745.
[9] M. Born, E. Wolf, *Principles of Optics: Electromagnetic Theory of Propagation, Interference and Diffraction of Light*, Cambridge University Press, Cambridge, England **1999**.
[10] A. Y. Borisevich, A. R. Lupini, S. J. Pennycook, *Proc. Natl. Acad. Sci. USA.* **2006**, *103*, 3044.
[11] J. Schindelin, I. Arganda-Carreras, E. Frise, V. Kaynig, M. Longair, T. Pietzsch, S. Preibisch, C. Rueden, S. Saalfeld, B. Schmid, J.-Y. Tinevez, D. J. White, V. Hartenstein, K. Eliceiri, P. Tomancak, A. Cardona, *Nat. Methods.* **2012**, *9*, 676.
[12] P. Thévenaz, U. E. Ruttimann, M. Unser, *IEEE Trans. Image Process.* **1998**, *7*, 27.
[13] A. R. G. Smith, K. H. Lee, A. Nelson, M. James, P. L. Burn, I. R. Gentle, *Adv. Mater.* **2012**, *24*, 822.
[14] M. A. Baldo, S. Lamansky, P. E. Burrows, M. E. Thompson, S. R. Forrest, *Appl. Phys. Lett.* **1999**, *75*, 4.
[15] W. Holzer, A. Penzkofer, T. Tsuboi, *Chem. Phys.* **2005**, *308*, 93.
[16] M. Gao, P. L. Burn, A. Pivrikas, *ACS Photonics.* **2021**, *8*, 2425.
[17] K. Yoshizaki, H. Yoshida, *Org. Electron.* **2015**, *20*, 24.
[18] M. Ikai, S. Tokito, Y. Sakamoto, T. Suzuki, Y. Taga, *Appl. Phys. Lett.* **2001**, *79*, 156.
[19] C. Chen, L. Hsu, P. Rajamalli, Y. Chang, F. Wu, C. Liao, M. Chiu, P. Chou, M. Huang, L. Chu, C. Cheng, *J. Mater. Chem. C.* **2014**, *2*, 6183.
[20] J. Jou, P. Wu, C. Lin, M. Wu, Y. Chou, H. Wang, S. Shen, *J. Mater, Chem.* **2010**, *20*, 8464.
[21] J. Jou, S. Kumar, A. Agrawal, T. Li, S. Sahoo, *J. Mater. Chem. C.* **2015**, *3*, 2974.
[22] C. W. Lee, J. Y. Lee, *Adv. Mater.* **2013**, *25*, 5450.